Indian Journal of Engineering & Materials Sciences
Vol. 27, October 2020, pp. 1027-1036

Mechanical and wear properties of Si_3N_4 reinforced titanium composites

Tugba Mutuk[a*] & Mevlüt Gürbüz[b]

[a]Department of Metallurgical and Materials Engineering, Ondokuz Mayis University, Samsun 55139, Turkey

[b]Department of Mechanical Engineering, Ondokuz Mayis University, Samsun 55139, Turkey

Received: 08 July 2019 ; Accepted: 08 May 2020

In the present study, Si_3N_4 reinforced titanium composites have been produced by the powder metallurgy method. The effect of various percentages of Si_3N_4 (0-9 wt. %) on the microstructure, density, hardness and compressive strength of titanium (It) composites have been investigated. After sintering at 1100 ^oC for 120 min., the mechanical properties have been significantly developed up to 3 wt. % Si_3N_4. The highest hardness and the greatest compressive strength have been obtained for 3 wt. % Si_3N_4 reinforced composite (698.5 HV and 1093 MPa) when compared to pure titanium (414.2 HV and 826 MPa). Si_3N_4 addition improved the wear properties of composites when compared to pure titanium. The lowest wear rate (1.36 x 10^{-5}, 2.75 x 10^{-5} and 5.15 x 10^{-5} mm^3 / Nm for 10 N, 20 N and 30 N, respectively) have been obtained for 3 wt. % Si_3N_4 reinforced titanium composite. Above this ratio, the properties of composites have deteriorated due to agglomeration tendency of Si_3N_4 powder. The scanning electron image, elemental mapping and line analyses confirm the uniform distribution of Si_3N_4 powder in Ti matrix. There has been no *in-situ* formed second phase of composite structure from the X-ray diffraction analyses.

Keywords: Titanium, Compressive strength, Microstructure, Silicon nitride, Powder metallurgy

1 Introduction

Studies on metal matrix composites such as aluminium (Al), magnesium (Mg) and titanium (Ti) have been increased over the past years. The reason for the fabrication of metal matrix composites (MMCs) is to protect the superior properties of the metal matrix and to improve its structural features[1]. Among them, Ti and its alloys are widely used in engineering fields such as aerospace, aviation, automotive and biomaterials industry due to their lightness, high strength and high corrosion resistance. However, better mechanical properties, high thermal conductivities, strong corrosion resistance and wear properties are needed in these fields. The fabrication of Ti in composite form reinforced with ceramic particles is an effective approach to provide higher mechanical, thermal / electrical and wear features[2-5].

In recent years, the researchers have been focused on to enhance Ti matrix composites (TMCs) reinforced with some ceramics such as SiC, Al_2O_3, B_4C, MgO, TiO_2, TiB, TiC, BN, Si_3N_4, etc. due to their high hardness, compressive strength and wear properties[3, 6-8]. Among them, Si_3N_4 particles have remarkable properties such as high compression/ impact strength, high-temperature strength, good thermal shock resistance, high corrosion resistance, high wear resistance and low creep properties[9].

In the last decades, most of the researches in the literature are related with especially on Si_3N_4 reinforced Al and Si_3N_4 reinforced SiC, AlN, TiN and ZrN[6, 10-13]. Şenel *et al.*[14], studied Al / Si_3N_4 composites which were fabricated by the powder metallurgy method. The Si_3N_4 powder was added to different percentages in the composite. The result showed that these reinforcement materials have a positive effect on the compressive strength of aluminum matrix composites. The effect of the Si_3N_4 whisker on aluminum composite properties under oxidation was published by Hu *et al* [15]. This process significantly increased the density, hardness and strength of the composites. The Si_3N_4-TiN composite was studied by Mussano *et al.*[16] as a bone interface material. Obtained data support the biocompatibility of the Si_3N_4-TiN.The corrosion and tribocorrosion behaviors are compared with traditional metallic biomaterial (Ti6Al4V). The Si_3N_4 / TiN ceramic composite was studied and compared by Monticelli *et al.*[17]. The test results showed that Si_3N_4 / TiN is a promising biomaterial in application because of its developed corrosion behavior. Blugan *et al.*[18] reported that Si_3N_4-TiN composite showed higher density, Young's modulus, the coefficient of thermal expansion, and

*Corresponding author: (E-mail: tugba.isitan@omu.edu.tr)

fracture toughness increased with increasing TiN content. Ahmad *et al.*[19] investigated Si_3N_4-TiN composites. In that work, composites were prepared by spark plasma sintering (SPS) process. Good micro-hardness and bending strength results were obtained.

As mentioned before, the studies in the literature are either on Ti-Si_3N_4 or Si_3N_4-ceramic (TiN, SiC, etc.) composites. Up to now, there have been performed a few studies on Si_3N_4 reinforced titanium composites which are at the conference level[20]. To our knowledge, there has been no report on detailed micro-structural and mechanical properties of the Si_3N_4 reinforced titanium composites.

Because of these considerations, pure Ti and Si_3N_4 reinforced Ti composites (0-9 wt. % Si_3N_4) were fabricated using the powder metallurgy (PM) method. Si_3N_4 addition effects on density, micro-hardness, compressive strength and microstructure of titanium composites have been evaluated and discussed.

2 Experimental procedures

2.1 Materials

In this work, the Ti powder was used as a matrix material which was supplied by Alfa Aesar (USA), with a purity of 99.5 % and diameters of less than < 43 micron. Si_3N_4 is 99 % purity, has 3.2 g/cm^3 and has an average particle size of < 1μm average particle size. The Si_3N_4 powder was purchased from UBE Industries (Japan).

Figure 1 (a & b) present the morphology of the Ti and Si_3N_4 powders. The particle size distributions of Ti and Si_3N_4 powders are shown in Fig. 1 (c) and (d), respectively. Ti contains both mostly spherical and rod - like particles and its size is under 43 μm. The average sizes of Si_3N_4 particles are approximately 0.8 μm.

2.2 Sample preparation

Si_3N_4 reinforcements of 0, 1, 3, 5, 7, 9 wt. % were mixed with pure Ti powder. Figure 2 shows the detailed schematic diagram of Ti-Si_3N_4 (Ti - SN)

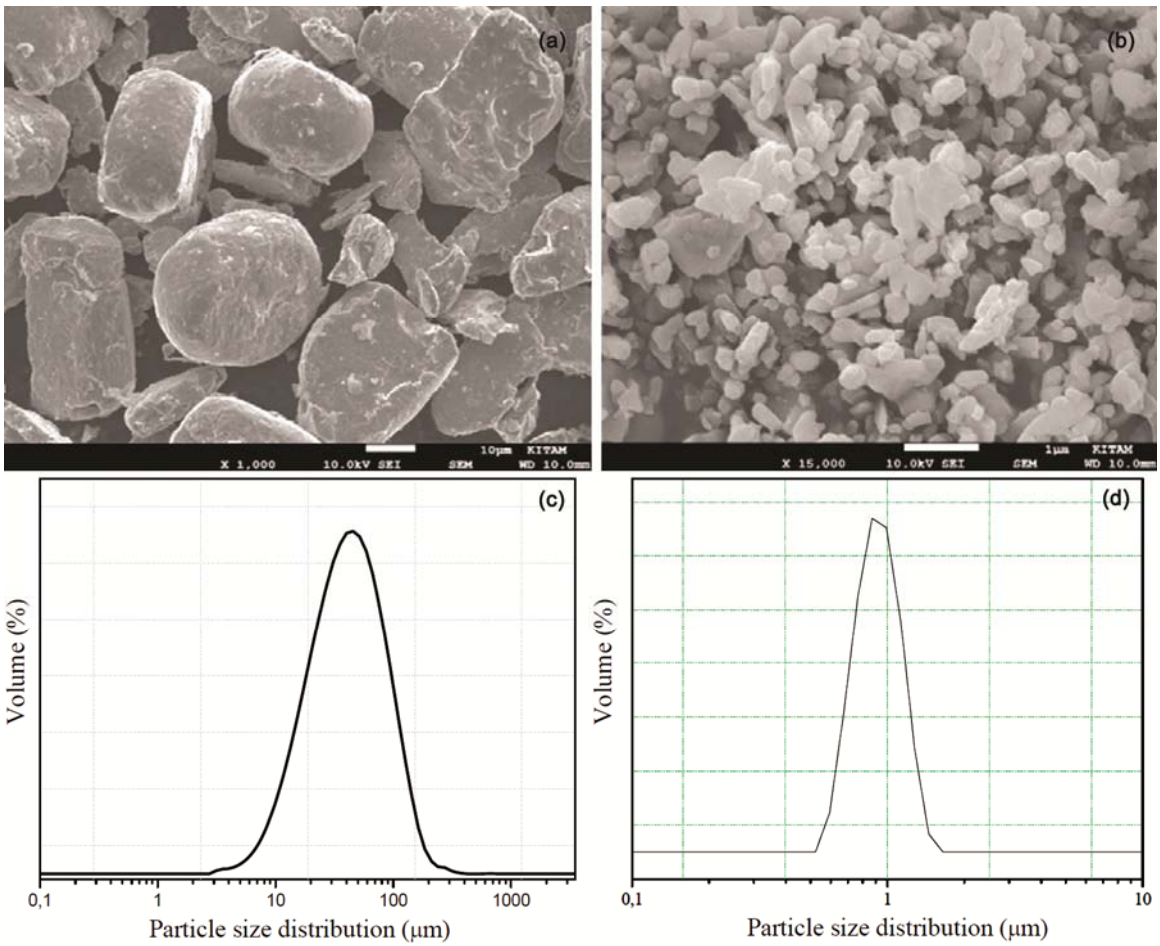

Fig. 1 — SEM image of (a) titanium, (b) Si_3N_4 powders, particle size distribution of (c) Ti and (d) Si_3N_4 powders.

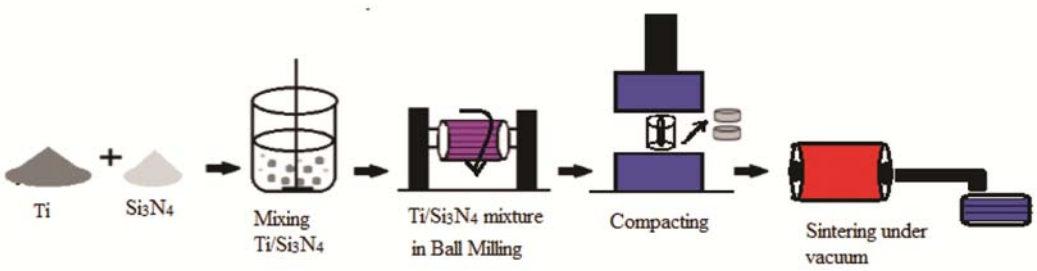

Fig. 2 — Schematic diagram of Ti-SN composites fabrication.

composite fabrication by PM method. Composite samples have been labeled in this study as follows: the 1wt. % Si_3N_4 reinforced composite labeled as Ti-SN1.

Firstly, both Ti and Si_3N_4 powders were mixed in ethanol using ultrasonic homogenizer roughly for twenty minutes and then the prepared powders were milled with a ball mill. Milling process was performed to produce powder mixtures Ti- Si_3N_4 at 100 rpm in a ball mill for 18 hours. YSZ (yttria stabilized zirconia) ball was used in the mill. After the milling process, the powders were compacted in a stainless steel mold with 10 mm diameter under 900 MPa to obtain disc and square samples. After shaping, materials were sintered under vacuum in the tube furnace at 1100 °C for 120 min. Selected sintering conditions were studied in detail by our previous paper which gives the effect of the sintering time and temperature on Ti properties[21].

2.3 Characterization

The microstructure and crystal phase of powder, composites were performed with a scanning electron microscope (SEM, Jeol JSM-7001F) and X-ray diffraction analysis (XRD, Rikagu Smartlab). Elemental mapping and line analyses were performed by using energy dispersive X-Ray (EDS) to confirm the existence of ceramic particles in Ti matrix. The size of Ti and Si_3N_4 powders were estimated by particle size analyzer (Malvern Mastersizer 3000). The apparent density and porosity were tested using Archimedes principles. The apparent density (ρ_c), percent of relative density (RD) (ρr (%)) and percent of porosity (P %) can be calculated as given in Eqs (1) to (3), respectively.

$$\rho_c = \left[\frac{W_K}{W_D - W_A}\right]\rho_w \quad ...(1)$$

$$\rho_r\,(\%) = \left(\frac{\rho_c}{\rho_t}\right) \times 100 \quad ...(2)$$

$$P(\%) = \left(1 - \frac{\rho_c}{\rho_t}\right) \times 100 \quad ....(3)$$

Here, W_K is the dry weight in the air, W_D is the saturated weight in the air, W_A is the hanging weight in water of saturated samples and ρ_W is the density of water[22].

The Vickers microhardness of composites was measured using hardness measurement device (HV-1000B) under a load of 500 g (HV 0.5) and waiting time of 15 s. The average values of (at least) six measurements conducted on different areas of each sample were considered. Compressive strength measurements were obtained using the universal testing machine (Mares Test- 10 tons). Five measurements were averaged for each composition with the compression rate of 10 mm min^{-1}. The wear behaviors of pure and composite samples were performed with a pin-on-disc test. The counterpart disc material was selected as X stainless steel. The wear properties were tested for 10, 20 and 30 N. The sliding speed and distance were selected as 200 rpm and 500 m, respectively. The trace of the surfaces after wear tests were examined by SEM analyses.

3 Results and Discussion

3.1 Density analysis, hardness and compressive strength of composites

Figure 3 (a) gives the apparent density of pure Ti depending on sintering temperature and time. The best sintering temperature and time obtained at 1100 ^oC for 120 min. The apparent density of Ti-SN composite was given after shaping and sintering (Fig. 3 (b) and Table 1). It is clearly shown that density of all Ti - SN composites significantly increase after sintering at 1100 ^oC for 2h. During sintering inter-particle bonding, diffusion and elimination of pore and pore size occurred due to the diffusion phenomena. The lowest energy required for the atomic transportation is called as "activation energy". The number of atoms with sufficient energy to move

at high temperatures can be obtained by the Arrhenius equation (Eq. (4))[23].

$$\frac{N}{N_0} = exp\left(-\frac{Q}{RT}\right) \quad ...(4)$$

where, N is a number of moving atoms, N_0 is a number of total atoms and Q is the activation energy. As the sintering temperature approaches the melting point, atom's movement increases due to the acceleration of sintering speed. Since the volume changes in the composite sample, the neck formation takes place between the particles. The apparent density of Ti-SN3 samples is increased from 4.17 ± 0.01 g / cm^3 (pure Ti) to 4.33 g / cm^3due to the sintering effect. Above 3 wt. % Si_3N_4 addition, the density was decreased to 4.17 ± 0.01 g/cm^3 due to the agglomeration tendency of Si_3N_4 particles. As given in Fig.1 (d), Si_3N_4 particle size is less than 1 µm which cause soft agglomeration and high friction between particles during shaping as a result of attractive forces. This disrupts the rearrangement of particles and flow behavior of Si_3N_4 in the mold. After 3 wt. % Si_3N_4, homogeneous distribution of Si_3N_4 between Ti grains are deteriorated due to agglomeration tendency. Therefore, restrictions of Si_3N_4 particle rearrangement and high friction during shaping cause the lower density and higher porosity[23-24].

Table 1 — Effect of the Si_3N_4 content on density and porosity of Ti composites.

Sample code	ρr (g/cm^3)	RD (%)-P (%) 1100 °C 120 min
Pure Ti	4.17	92.7 – 7.3
Ti- SN1	4.31	96- 4
Ti- SN3	4.33	97 – 3
Ti- SN5	4.21	94.6 – 5.4
Ti- SN7	4.24	95.7 – 4.3
Ti- SN9	4.14	94 - 6

Figure 4 demonstrates the Vickers hardness of sintered Ti-SN composites at 1100 °C for 120 min.

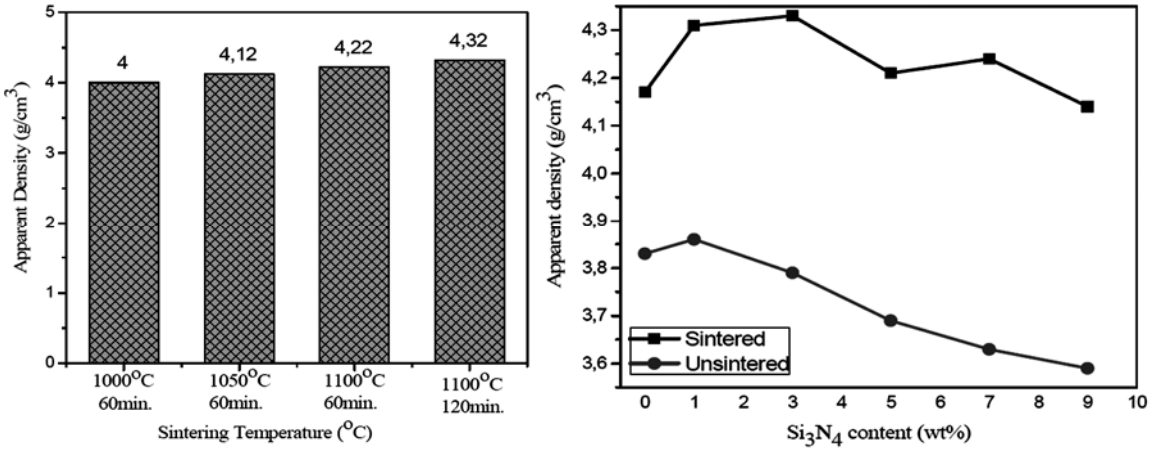

Fig. 3 — The apparent density of (a) pure Ti with temperature and time and (b) Ti composites with Si_3N_4 content.

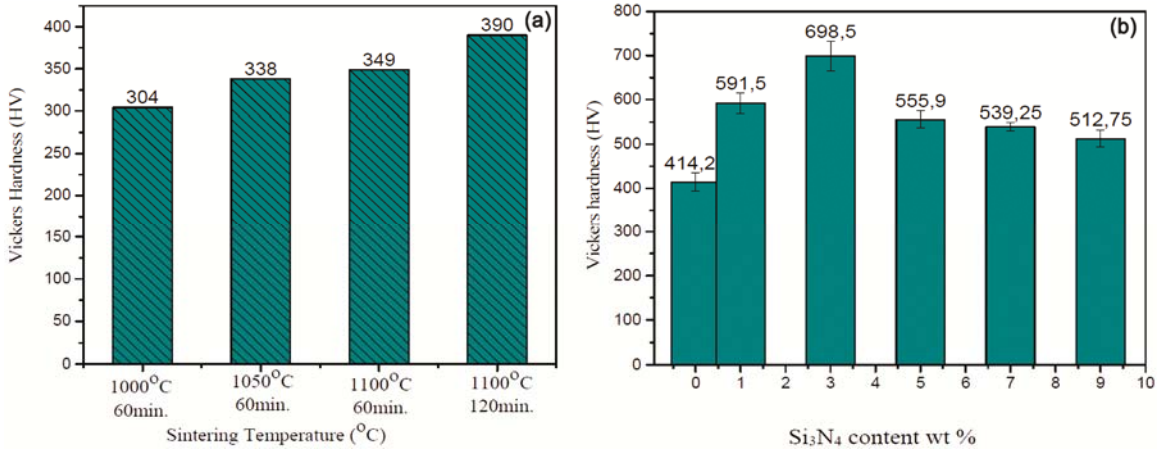

Fig. 4 — Vickers hardness variation of (a) pure Ti for different temperature and time (b)Ti-SNcomposites for various Si_3N_4 amount.

Figure 4 (a) illustrates the Vickers hardness of pure Ti depending on the sintering temperature and time. The highest hardness is measured at 1100 °C for 120 min. Up to 3 wt. % Si_3N_4 addition to Ti has a significant effect to increase the hardness of composites (Fig. 4 (b)). The highest hardness was measured 699 HV for 3 wt. % Si_3N_4 reinforcement when comparing with pure Ti (414 HV). It can be explained with uniformly dispersed Si_3N_4 and strong neck formation after sintering. Moreover, homogeneously dispersed Si_3N_4 creates more contact area between Ti particles. The dispersed Si_3N_4 restricts the grain growth and suppresses the dislocation movement during the mechanical test. Furthermore, Eq. (5) can explain the improvement of hardness for Si_3N_4 reinforced Ti composites. The dislocation strengthening mechanisms control the hardness of composites. Si_3N_4 increased the dislocation density in Ti structure due to its small size. As given in Eq. (5), hardness (H) depends on the square root of dislocation density.

$$H = h\sqrt{Dt} + \alpha G b\sqrt{\rho} \quad ...(5)$$

where h, α, G are material constant, b is Burgers vector and ρ is the dislocation density[21-26]. Therefore, the composite hardness increases at a certain sintering temperature (1100 °C) and optimum amount of Si_3N_4 (3 wt. %). Si_3N_4 content causes agglomeration and it led to weak interphase with Ti and Si_3N_4. This led to higher porosity, lower density and less hardness.

The compressive strength graph of Si_3N_4 reinforced Ti composites are given in Fig. 5 (a). It is clearly shown that Si_3N_4 up to 3 wt. % has a positive effect on compressive behavior. Also, the ductility of the Ti composites reduces with Si_3N_4 addition. The ultimative compressive strength (UCS) of composites Ti-SN1 and Ti-SN3 reached up to 925 MPa and 1093 MPa, respectively which are higher than the sintered (825 MPa) pure Ti (Fig. 5 (b)). UCS of Ti composites is decreased to 360 MPa with increasing Si_3N_4 amount. The increase in strength of composite can be explained by dislocation density, load transfer and crack deflection strengthening mechanisms. The Si_3N_4 act as a barrier during sintering which causes to increase in dislocation density. The load transfer mechanisms have a main role during the compression test. Higher compression behavior is one of the most important property of ceramics. Therefore, a certain amount of Si_3N_4 provides a better compressive strength to the Ti composites. The cracks initiate and propagate with increasing load during the test. The ceramic particles act as a barrier to propagate the cracks. When the cracks close to the ceramic particles, the crack deflection takes place which causes the reduction of crack propagation energy[27-28,18]. Theoretically, Eqs (6) and (7) give the mechanical properties and reinforcement element relations, respectively. From Eq. (6), Si_3N_4 particles lead to decreasing the distance between particles.

$$\lambda = \frac{[4(1-f)r]}{3f} \quad ...(6)$$

where λ is the distance between the reinforcement particles, f is the volume fraction of reinforced particles and r is the radius of ceramic particles. From the Eqn. (7), shear stress is inversely proportional to λ:

$$\tau_0 = \frac{Gb}{\lambda} \quad ...(7)$$

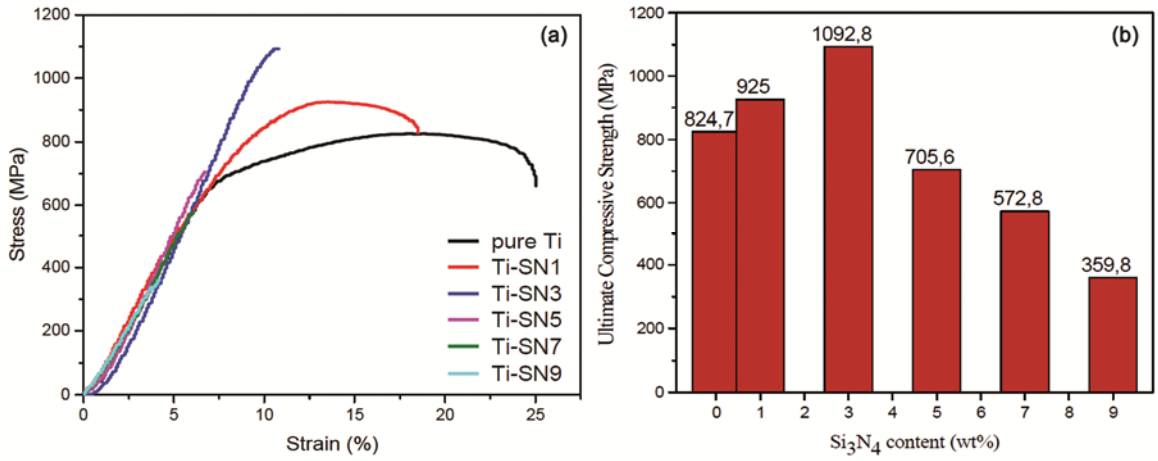

Fig. 5 — Compressive strength behaviour of (a) pure Ti and Si_3N_4-reinforced composites and (b) UCS of the sample.

where τ_0, G, b, and λ stands for the shear stress, shear module, Burger's vector and distance between the GNP particles, respectively. From these equations, it can be understood that as the distance between particles decreases, the shear stress increases. At the same time, the strength of composite improves[29]. These equations are valid for optimum conditions such as more uniform particle dispersion without agglomeration and matrix grain growth etc. They are depend on the particle size, shape, temperature etc. But in real conditions, the control of these parameters can not possible e.g. when used small particles, and it tends to large agglomeration due to electrostatic forces between particles. These also led to a partially agglomerated non stable zone, which causes a negative effect on composite properties. Moreover, increasing the reinforcement element led to the changing sintering ability of matrix materials. Uniform dispersed particles provide more contact between the particles. But increasing the reinforcement element has a negative effect on the sintering ability of matrix due to the more porosity between agglomerated hard ceramic particles.

The XRD analyses of raw Ti and Si_3N_4 powders are present in Fig. 6 (a). These main diffraction patterns are good guides to determine the crystal structure of the composites and in-situ formed undesired second phases such as TiN or Ti - Si formation after sintering. The XRD patterns of Si_3N_4 reinforced Ti composites after sintering were given in Fig. 6 (b). The Si_3N_4 and Ti peaks are clearly observed without undesired second phases. Also, the worn surfaces of the samples were characterized with XRD. The diffraction patterns were similar as fabricated other samples.

Figure 7 (a-f) gives thelow and high magnification SEM images of the pure Ti, Ti - SN3 and Ti - SN7 composites. From the SEM images, the morphology of pure Ti and Ti-SN3 have strong particle bonding and necking between Ti grains. Si_3N_4 particles are located at Ti grain boundaries which distributed homogeneously. Above the 3 wt. % Si_3N_4 content, the microstructure includes more porosity due to the agglomeration and higher content of ceramic particles. The SEM images confirm the density and hardness results.

Figure 8 illustrates the stereo microscopy images and elemental maps for Ti - SN3. In Fig. 8 (a-b), highly dense composites are shown from both polished and fractured surface. As shown by EDX mapping (Fig. 8 (c-e), the main elements in the composite are Ti (green color), Si and N from Si_3N_4 (blue and red color). Si_3N_4 has uniform distribution at Ti grain boundaries.

To confirm the existence of Si_3N_4 at Ti grain boundary, line analyses were performed at the fracture surface of composite (Fig. 9). Line analysis confirms that Si_3N_4 exist at the Ti grain boundary. The Ti signals are reduced when they are close to the Si_3N_4 particles at the grain boundary.

The wear behaviours of Ti composites were evaluated by using a pin-on-disc wear test unit. The sliding distance (L) was calculated according to Eq. (8),

$$L = 2\pi Rnt \quad ...(8)$$

$$\Delta V = \frac{\Delta m}{\Delta \rho} \quad ...(9)$$

$$W = \frac{\Delta V}{P * L} \quad ...(10)$$

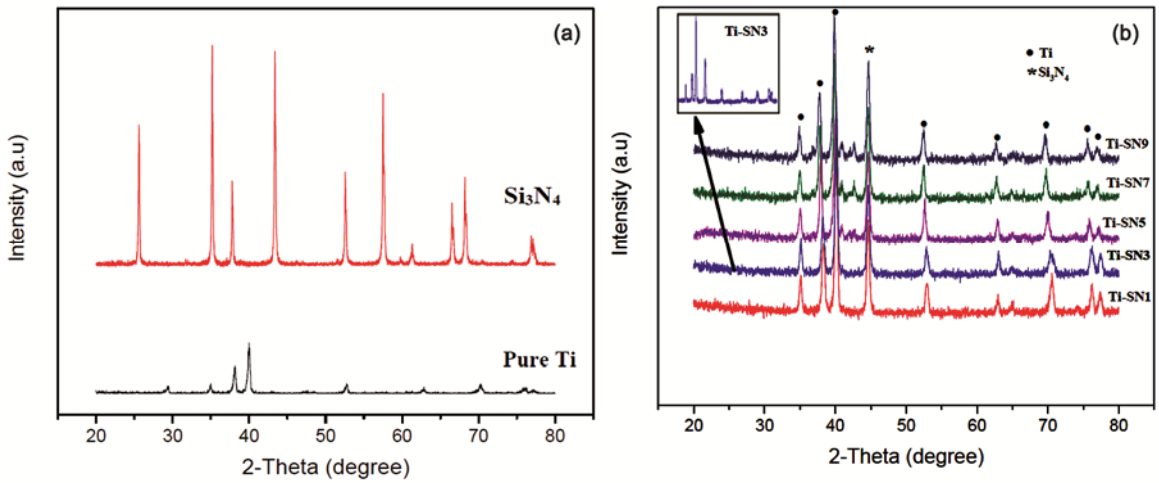

Fig. 6 — XRD plot of (a) raw materials (Ti-Si_3N_4) and (b) and their composites.

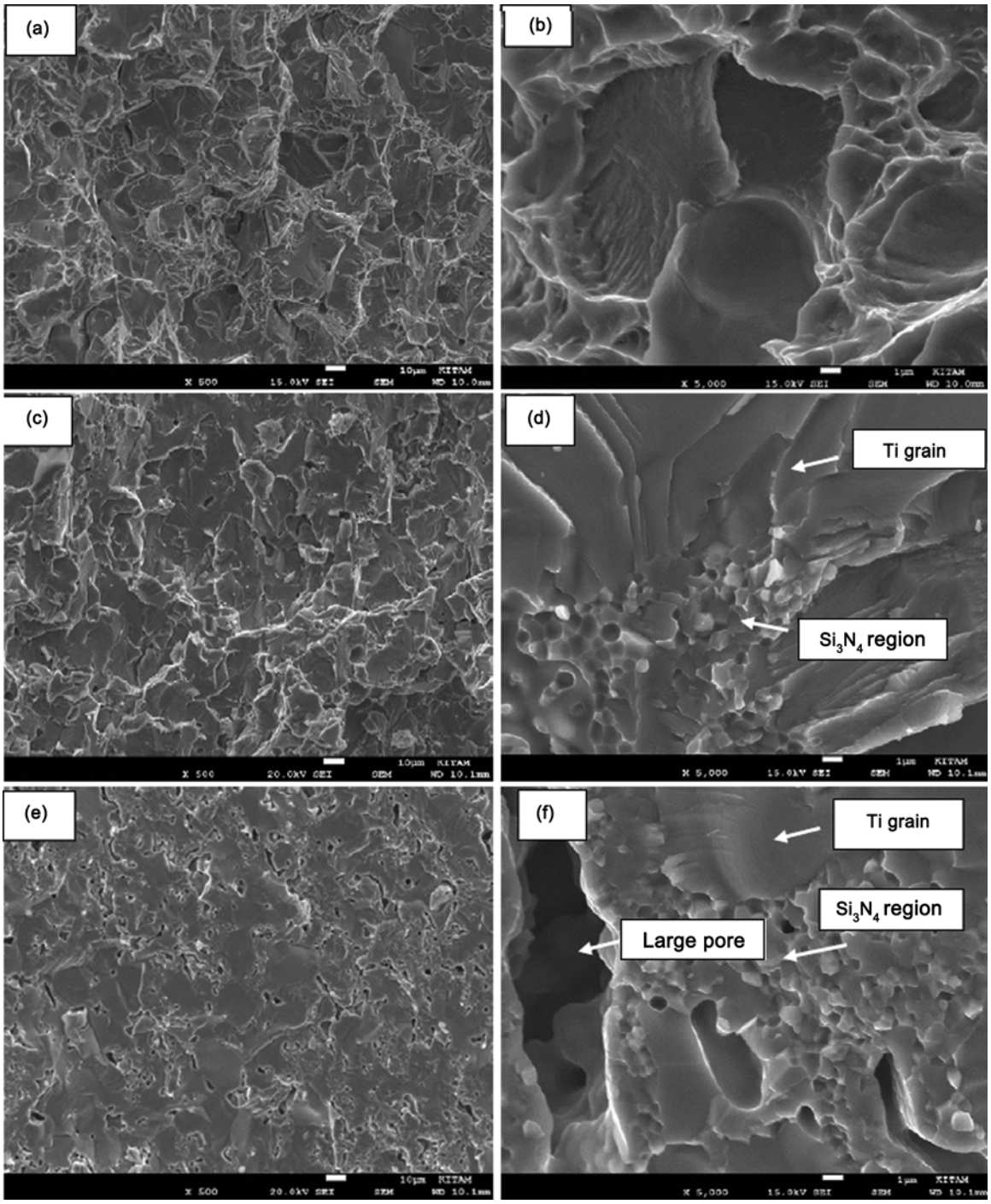

Fig. 7 — Low and high magnification images of (a-b) pure Ti, (c-d) 3 wt. % Ti-SN and (e-f) 7 wt. % Ti-SN composite.

where L is the sliding distance (500 m), R is the radius of counterpart disc (20 mm), n is the number of revolutions (200 rpm) and t is the testing time (20 min.). The volume changes of worn samples (ΔV, Eq. (9)) were measured using by mass loss (Δm) and density of composite (ρ). The wear rates (W) of composites were calculated as given in Eq. (10), where W, P is the wear rate (mm^3 / (Nm)) and applied load (N), respectively[30].

The mass loss (Δm) and wear rate (W) with various loads for 3 wt. % Si_3N_4 reinforced Ti composites were shown in Fig. 10(a-b). The lowest mass loss and wear rate (Δm = 0.3 mg, W = 1.36 x 10^{-5} mm^3 / (Nm)) were observed under 10 N load when compared pure

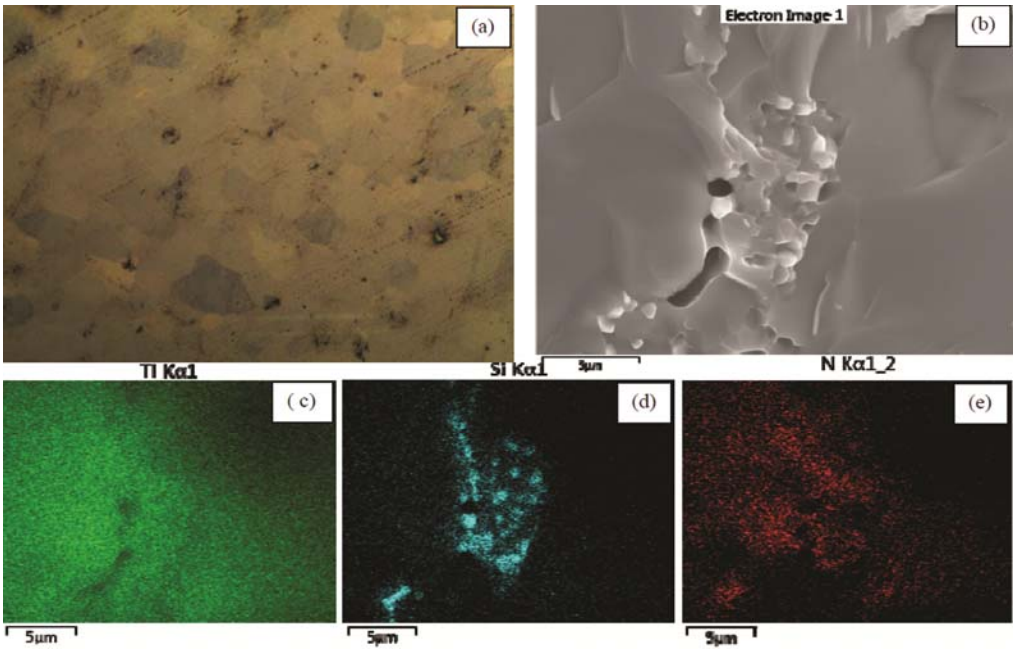

Fig. 8 — Stereo images of polished surface (a) SEM and (b-e) elemental mapping of Ti-SN3 composites.

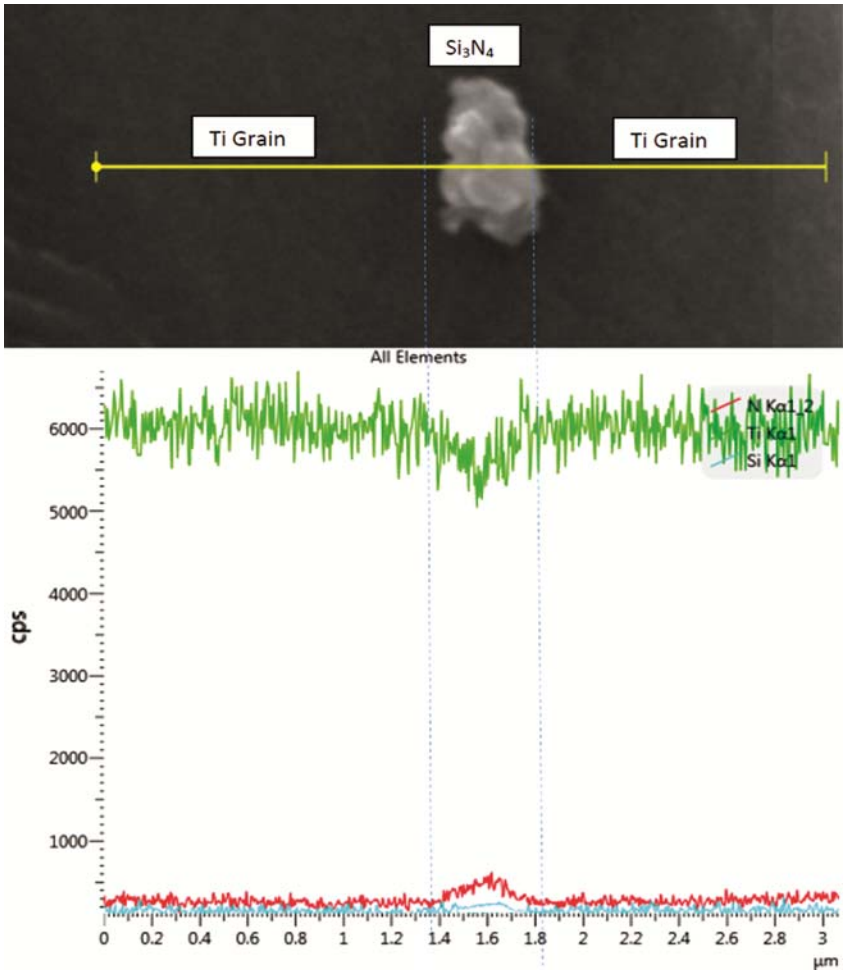

Fig. 9 — Line analyses of Ti-SN3 composites.

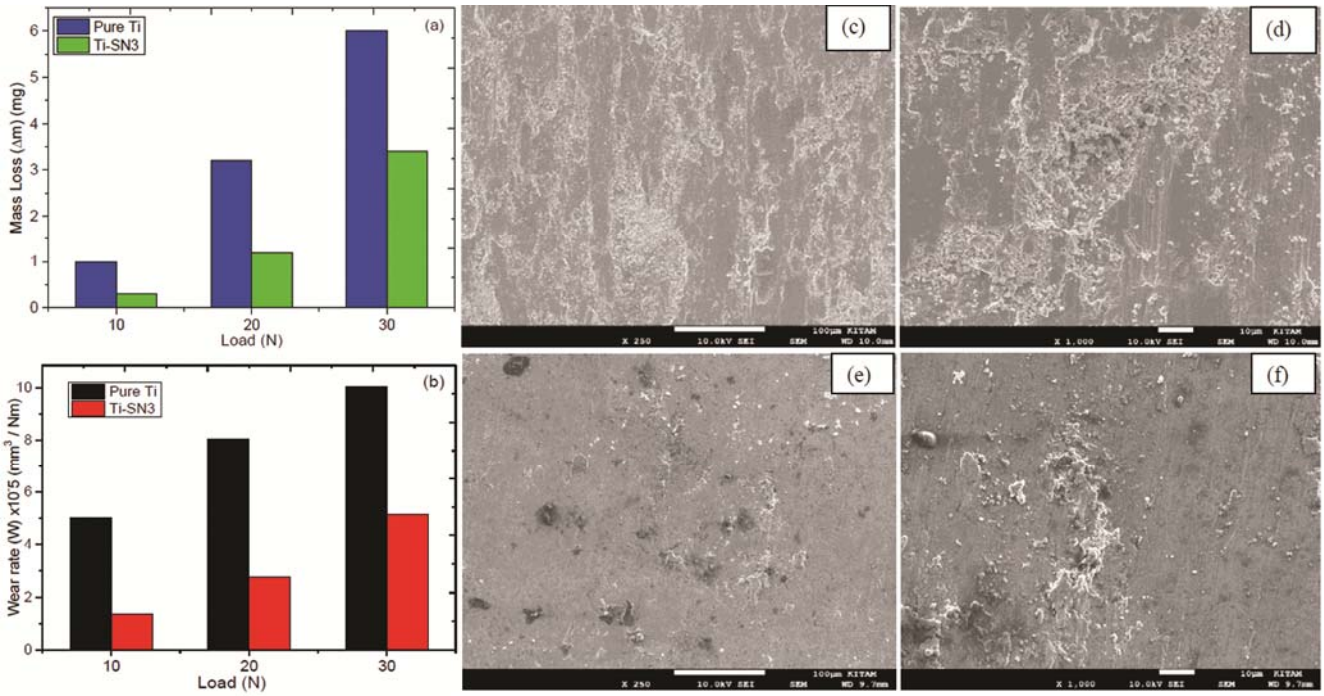

Fig. 10 — (a-b) Mass loss and wear rate and (c-f) low and high magnification SEM images of worn surface for pure Ti and Ti-SN3 composite.

Ti (Δm =1 mg, W=5.02 x 10^{-5} mm^3 / (Nm)).The wear rate was increased with increasing load as expected. SEM images of the worn surfaces under maximum load (30 N) for pure Ti and Ti-SN3 composites were given in Fig. 10 (c-f). The images clearly show that pure Ti samples include more damage on the worn surfaces. The most serious damage and the deepest grooves were observed in pure titanium. On the other hand, less damage was detected on the surface of Ti-SN3 composite. Moreover, we examined higher ratios Si_3N_4 added samples which has a more defected morphology as the same the pure Ti samples. It includes a more deteriorated area with increasing agglomeration of the Si_3N_4. These agglomerated particles dispersed during the wear test between sample and counter disc. Therefore it acts as abrasive particles and causes the reduction of wear resistance property.

4 Conclusions

Fabrication of Ti-SN composites were performed for various Si_3N_4 content by using PM method. The effects of Si_3N_4 addition on the density, Vickers hardness, compressive strength and microstructure of composites have been examined.

(i) The best result was obtained at 1100 ^oC 120 min. The highest density and Vickers hardness values were obtained for 3 wt. % Si_3N_4 content. These values are 4.33 g / cm^3 and 698 HV, respectively.

(ii) The hardness of Ti-SN composites increased from 414 HV (pure Ti) up to 3 wt. % Si_3N_4 content (Ti-SN3) 698 HV. It reduces with the addition of Si_3N_4 above 3 wt. % due to the agglomeration tendency of Si_3N_4 powders.

(iii) The highest compressive strength was performed for 3 wt. % Si_3N_4 reinforced composites (1093 MPa) comparing with pure Ti (826 MPa).The minimum wear rates (1.36 x 10^{-5}, 2.75 x 10^{-5} and 5.15 x 10^{-5} mm^3 / (Nm) for load of 10 N, 20 N and 30 N) were measured for 3 wt. % Si_3N_4 reinforced Ti samples.

(iv) According to SEM results, bonding between the particles and good neck formation were observed at 1100 ^oC for 120 min.

(v) The SEM analyses confirmed the Si_3N_4 distributions in the Ti matrix. Si_3N_4 was detected along the Ti grain boundaries. Further studies can be conducted on this study and this study will contribute to them.

Acknowledgment

The author(s) disclosed receipt of the following financial support for the research, authorship, and publication of this article: This study is fully

supported by The Scientific and Technological Research Council of Turkey (TUBITAK) (Project No: 217M154). Also, the authors are pleased with the partial support for this study from Ondokuz Mayıs University, Scientific Research Project Department under the grants (PYO.MUH.1902.15.001 and PYO.MUH.1906.14.006).

References

1 Qian M & Froes FH, (Copyright Elsevier Inc.) Oxford, UK, 2015, ISBN: 9780128009109
2 Mu XN, Zhang H M, Cail H N, Fan Q B, Wu Y, Fu Z J & Wang QX, ICCMME 201, *AIP Conf Proc*, 1 (2017).
3 Song Y, ChenY, Li W, Wang G, Zhao D & Liu X B, *Mater Des*, 109 (2016) 256.
4 Bodunrin M, Alaneme K K & Chown L H, *JMR & T*, 5(4) (2015) 434.
5 Shirvanimoghaddam K, Hamim S U, Akbari M K, Fakhrhoseini S M, Khayyam H, Pakseresht A H, Ghasali E, Zabet M, Munir K S, Jia S, Davim J P & Naebe M, *Compos Part A*, 92 (2017) 70.
6 Sharma P, Sharma S & Khanduja D, *J Asian Cer Soc*, 3 (2015) 352.
7 Cao Z, Wang X, Li J, Wu Y, Zhang H, Guo J & Wang S, *J Alloy Compd*, 696 (2017) 498.
8 LI S, Kondoh K, Imai H, Chen B, Jia L & Umeda J, *Mater Sci Eng A*, 628 (2015) 75.
9 Tang X, Li Y, Cheng X & Zhang Y, *Ceram Int,*44 (2018) 10322.
10 Xiu Z Y, Chen G, Wu G, Yang W & Liu Y, *Trans Nonferrous Met Soc China*, 21 (2011)285.
11 Jiang Y, Wu L E &Sun W Z, *Rare Metals*, 34(2) (2015) 95.
12 Yin L, Xu Y, Huang Z, Liu Y, Fang M & Baolin L, *Powder Technol*, 246 (2013) 677.
13 Gao L, Li J, Kusunose T & Nihara K, *J Eur Ceram Soc,* 24 (2004) 381.
14 Şenel M C, Gürbüz M & Koç E, *J Mater Sci,* 5(4) (2017) 95.
15 Hu Z S, Geng H R, Hou X Q & Leng J F, *Key Eng Mater,* 575-576 (2014) 50.
16 Mussano F, Genova T, Rivolo P, Mandracci P, Munaron L, Faga M G & Carossa S, *J Mater Sci*,52 (2017) 467.
17 Monticelli C, Zucchi F & Tampieri A, *Wear,* 266 (2009) 327.
18 Blugan G, Hadad M, Janczak-Rusch J, Kuebler J & Graule T, *J Am Ceram Soc,* 88(4) (2005) 926.
19 Ahmad N & Sueyoshi H, *Mater Res Bull,* 46 (2011) 460.
20 Dougherty T, Xu Y & Hanizan A, TMS, Annual Meeting Supplemental Proceedings (The Minerals, Metals & Materials Society) (2016)
21 Gürbüz M & Mutuk T, *J Compos Mater,* 52(4) (2018) 543.
22 Aatthisugan A R, Rose D & S Jebadurai, *J Mag All*, 5 (2017) 20.
23 Rahimian M, Ehsani N, Parvin N & Baharvandi H, *J Mater Process Technol,* 209 (2009) 5387.
24 Varol T & Canakci A, *Metals Mater Int,* 21(2015) 704.
25 Wang J, Li Z, Fan G, Pan H, Chen Z & Zhang D, *Scripta Mater,* 66 (2012) 594.
26 Chen L Y, Konishi H, Fehrenbacher A, Ma C, Xu Q, Choi H, Xu H, Pfefferkorn F E & Li XC, *Scripta Mater,* 67 (2012) 29.
27 Hu Z, Tong G, Nian Q, Xu R, Saei M, Chen F, Chen C, Zhang M, Guo H & Xu J, *Compos Part B,* 93(2016) 352.
28 Liu Y, Huang J & Li H, *J Mater Chem B*, 13 (2013)1826.
29 Latief F H & Sherif E S M, *J Ind Eng Chem,* 18 (2012) 2129.
30 Şenel M C,Gürbüz M & Koç E, *Mater Sci Tech*, 34 (2018)1980.